Bioresource Technology 360 (2022) 127570

Contents lists available at ScienceDirect

Bioresource Technology

journal homepage: www.elsevier.com/locate/biortech

High-purity lignin fractions and nanospheres rich in phenolic hydroxyl and carboxyl groups isolated with alkaline deep eutectic solvent from wheat straw

Xin Yue [a], Terhi Suopajärvi [a], Shirong Sun [b], Otto Mankinen [c,d], Atte Mikkelson [e], Harri Huttunen [f], Sanna Komulainen [c], Idamaria Romakkaniemi [g], Juha Ahola [g], Ville-Veikko Telkki [c], Henrikki Liimatainen [a,*]

[a] Fiber and Particle Engineering Research Unit, University of Oulu, P.O. Box 4300, 90014 Oulu, Finland
[b] School of Chemical Engineering and Light Industry, Guangdong University of Technology, 510006 Guangdong, China
[c] NMR Research Unit, University of Oulu, P.O. Box 4300, 90014 Oulu, Finland
[d] Department of Diagnostic Radiology, Oulu University Hospital, 90014 Oulu, Finland
[e] VTT Technical Research Centre of Finland, Vuorimiehentie 3, 02150 Espoo, Finland
[f] Unit of Measurement Technology MITY, Teknologiapuisto PL 127, 87400 Oulu, Finland
[g] Chemical Process Engineering Research Unit, University of Oulu, P.O. Box 4300, 90014 Oulu, Finland

HIGHLIGHTS

- Alkaline DES consisting of K_2CO_3 and glycerol was developed for lignin extraction.
- Sequential fractionation facilitates the production of high-purity DES lignin.
- Lignin rich in Ar–OH (9.60 mmol/g) and –COOH groups (2.52 mmol/g) was obtained.
- Alkaline DES was conducive to reducing the β-O-4 linkages of lignin.

GRAPHICAL ABSTRACT

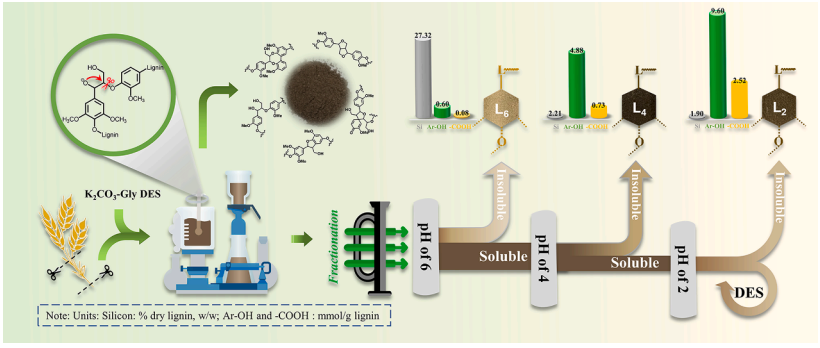

ARTICLE INFO

Keywords:
Alkaline deep eutectic solvent
High-purity lignin
Sequential acid fractionation
Phenolic hydroxyl
Wheat straw

ABSTRACT

A combined pretreatment based on alkaline deep eutectic solvent (DES) of K_2CO_3 and glycerol and sequential acid fractionation was developed to extract reactive lignin from wheat straw biomass. This process exhibited excellent purification performance in lignin isolation, and the lignin fractionated at low pH displayed high reactivity, having hydroxyl and carboxyl groups up to 9.60 and 2.52 mmol/g, respectively. Silica was selectively separated and removed during the precipitation stage, avoiding the "silica interference". Moreover, DES-lignin nanospheres created by self-assembly using lignin fractions obtained by acid precipitation possessed a high zeta potential, large particle size and high content of hydrophilic groups. Overall, the findings related to the

* Corresponding author.
E-mail address: henrikki.liimatainen@oulu.fi (H. Liimatainen).

https://doi.org/10.1016/j.biortech.2022.127570
Received 27 May 2022; Received in revised form 28 June 2022; Accepted 29 June 2022
Available online 3 July 2022

dissociation mechanism and fractionation of reactive lignin during alkaline DES pretreatment and the acid sequence precipitation are crucial for facilitating lignin valorization in high-added value products.

1. Introduction

Lignin, one of the three major components of lignocellulosic biomasses, is the most abundant renewable resource of aromatic biopolymers. It is regarded as a highly intriguing raw material for the synthesis of various bio-based functional materials and has extensively been utilized in the design of valuable green products (Shuai et al., 2016). Currently, the dominant source of technical lignin is the kraft pulping process, in which the lignin is a by-product of the cellulose pulp and is mainly used as energy supply in the recovery boiler. However, there are also several other biorefinery concepts producing technical lignins with different physicochemical properties, depending on the biomass source, isolation method, and processing conditions. The common challenge of all these approaches is the further efficient utilization of lignin, mainly because of its heterogeneous and complicated structure (Brandt et al., 2015; Sethupathy et al., 2022).

As an alternative technique to conventional alkaline pulping, ionic liquids (ILs) have been used to extract lignin from lignocelluloses owing to their effective fractionation performance, thermal stability, and easy operation. However, their industrial applications are still limited due to their high costs and difficulties related to chemical recovery and recycling (Ji and Lv, 2020). Deep eutectic solvents (DESs) are a relative new class of green solvents, which are typically prepared by complexation of hydrogen bond donors (HBD) and hydrogen bond acceptors (HBA), to result in versatile solvent systems having many similar characteristics to ILs. However, DESs can be synthesized from inexpensive components, and some systems can be recycled and possess good biodegradability (Zhou et al., 2021). Recently, acidic DESs prepared by mixing choline chloride (ChCl) and organic acids (e.g., lactic acid, oxalic acid, maleic acid, and *p*-toluene sulfonic acid) have been harnessed for lignin extraction from lignocellulose to extract high-purity lignin with high yield (Lou and Zhang, 2022; Shen et al., 2020). However, the condensation reaction of lignin during acidic extraction causes its molecular weight to increase and the content of functional groups (such as − OH and carbonyl groups) to decrease (Jasiukaitytė-Grojzdek et al., 2012). Additionally, neutral DESs have also been applied to extract lignin from lignocellulosic biomass. However, their pretreatment efficiency is often low and harsh reaction conditions are required (Chen et al., 2020). Consequently, DESs having alkaline characteristics are highly appealing for the lignin extraction from plant biomasses in industrial conditions, although they have received less attention.

From the industrial perspective, the precipitation of lignin after its extraction is crucial to obtain solid fractions whether using traditional alkaline methods or applying novel solvent systems such as DESs (Yan et al., 2020). pH-induced precipitation has been used for the preparation of lignin nanoparticles (LNPs) from pulping black liquor to achieve lignin classification (Yan et al., 2020). Similarly, alkaline DESs could also be used for lignin classification based on DES extraction followed by pH adjustment. However, there is scarcity of information related to the role of pH-induced precipitation in the characteristics of lignin fractions (such as purity, structure, intra- and intermolecular interactions, aggregation process, etc.), especially under the alkaline DES system.

This work aims to elucidate the isolation and fractionation processes of lignin during combined alkaline DES pretreatment and acidic precipitation. Afterwards, the formation of lignin nanospheres from different fractions by self-assembly is addressed. A detailed comparison of the structural and chemical characteristics of different lignin fractions were investigated to confirm the molecular properties–structure relationship. In addition, the delignification mechanism and aggregation procedures during the alkaline DES pretreatment were studied in detail. In the present work, the described refined system provides a new avenue to achieve silicon-free lignin that homogenize the physicochemical properties and improve the chemical reactivity of lignin. The information acquired is of vital importance to explore its potential valorization in lignin-based biohybrid materials.

2. Materials and methods

2.1. Materials

Wheat straw was harvested from Chile and was dried and ground to pass through 1-mm screen. The straw sample consisted of 22.1 wt% of lignin, 39.8 wt% of cellulose, 18.0 wt% of hemicelluloses, 4.5 wt% of ash, and 15.6 wt% of others. All reagents used in this study were commercially purchased and used as received. Deionized water (DIW) was used throughout the experiments.

2.2. Fractionation of lignin using DES extraction and sequential acid precipitation

Alkaline DES was prepared by mixing glycerol and K_2CO_3 with a molar ratio of 5:1 (Suopajärvi et al., 2020). The mixture was heated with an oil bath at 100 °C under moderately stirring until a transparent liquid (K_2CO_3-Gly DES, pH ~ 12.9, viscosity ~ 17,613 cP, onset temperature ~ 268.4 °C) was obtained (Lim et al., 2019). Approximately 10 g of wheat straw (based on oven-dried mass) was transferred into K_2CO_3-Gly DES at 3 wt%. The mixture was then stirred at 100 °C for 16 h followed by the addition of 100 mL ethanol and filtration to stop the reaction. The K_2CO_3-Gly DES filtrate was further processed using a sequential acid precipitation to obtain three different DES lignin fractions (L_6, L_4, and L_2) and the experimental procedure is described in detail (Fig. 1). The alkaline DES filtrate was acidified directly to pH 2 using HCl (one-step precipitation), and the lignin precipitate after centrifugation was denoted as unfractionated lignin L_O. It is likely that also higher solids loading could be used in the DES treatment which can reduce the processing costs and decrease the amount of used chemicals. Moreover, the remaining DES liquid can be recycled by separating the EtOH with a rotary evaporator and adjusting the DES properties by K_2CO_3 make-up. The properties of L_O were described in detail in our previous study (Yue et al., 2020). The insoluble DES lignin fractions L_O, L_6, L_4, and L_2 were washed several times with DIW to neutral pH and freeze-dried for further analysis.

2.3. Preparation of lignin nanospheres

The unfractionated DES lignin (L_O) and lignin fractions (L_6, L_4, and L_2) were dissolved into THF at a concentration of 10 mg/mL. Subsequently, the solutions were filtered through a 0.45 μm syringe filter and were added to the dialysis membrane tube (Spectra/Por® 3 Standard RC Tubing, MWCO 3.5 kD, Spectrum Labs, USA). The membrane was immersed in an excess of DIW while stirring slowly. Periodically replaced the water, and dialysis was carried out for 24 h. The dialysis products were recovered by centrifugation (10,000 rpm) and then freeze-dried to obtain solid lignin nanospheres. The produced nanospheres were denoted as LNP_O, LNP_6, LNP_4, and LNP_2, respectively.

2.4. Characterization

Structural and chemical characteristics of the lignin fractions were investigated by high-performance anion-exchange chromatography (HPAEC, Dionex ICS-5000, CarboPac PA20 column, USA), elemental analysis (CHNS/O FLASH 2000 Series, Thermo Scientific, USA), X-ray

photoelectron spectroscopy (XPS, ESCALAB 250Xi spectrometer, Thermo Fisher Scientific, UK), X-ray fluorescence spectrometer (XRF, Axios^{mAX} PANalytical, UK) Fourier transform infrared spectroscopy (FT-IR, Nexus-870, Thermo Nicolet, USA) with a spectral range from 4000 to 400 cm^{-1} at a spectral resolution of 4 cm^{-1}, gel permeation chromatography (GPC, Agilent 1260 series chromatograph, Agilent Technologies, USA), thermogravimetric analysis (TGA, thermogravimetric analyzer, Netzsch STA 449F3, Germany), and nuclear magnetic resonance (NMR, 14.1 T Bruker Avance III 600 spectrometer, Bruker, Germany) techniques. Dynamic light scattering (DLS, Zetasizer Pro instrument, Malvern Panalytical Ltd, UK) was used to determine the average zeta potential and particle size of DES-lignin nanospheres fabricated from different lignin fractions. The micromorphologies of the LNPs were observed by field emission scanning electron microscope (FESEM, Zeiss Sigma HD VP, Oberkochen, Germany) and transmission electron microscope (TEM, JEOL JEM-2200FS, Japan). All the detailed procedures were performed according to previous experimental description (Brandt et al., 2015; Yue et al., 2020).

3. Results and discussion

3.1. Purity and yield of alkaline DES-extracted lignin and acid-precipitated fractions

Table 1 presents the quantitative compositional analysis of lignin samples, i.e., the contents of Klason lignin (acid-insoluble lignin, AIL), acid-soluble lignin (ASL), ash, monosaccharides, and polysaccharides. The purity of the L_6 sample was ~ 17 wt%, which was quite different from that of the L_2 sample (~91 wt%), probably because the ash in L_6 accounted for ~ 62 wt%, approximately 30 times more than the ash content in L_2. The alkaline soluble silicates, which exist inherently in wheat straw and are a common problem in alkaline cooking, precipitated once the DES extract was acidified (Deniz et al., 2004). Consequently, the purity of lignin fractions improved, and the ash content decreased gradually as the precipitation progressed from pH 6 (L_6) to pH 2 (L_2). Simultaneously the great majority (59 wt%) of Lo was precipitated in pH 6 condition, while the dissolved fraction was further fractionated with stronger acid solutions: 26- wt% (pH 4) and 15- wt% (pH 2) solid lignin fraction, respectively (see supplementary material).

The coprecipitation of carbohydrates was minor, the total carbohydrate content being < 3.3 wt% with all lignin samples and the detected monosaccharides being mainly attributed with hemicelluloses (xylose, arabinose, galactose, and mannose) (Huijgen et al., 2014). Another important observation was the rather low amounts of polysaccharides (≤2.91 wt%), further confirming that chemical linkages between lignin and hemicellulose in lignin fractions were efficiently cleaved during alkaline DES treatment.

The overall view of characteristic functional groups of lignins are elucidated by the FT-IR spectra (see supplementary material). All the lignin samples preserved the basic skeleton structure of phenylpropane, which was assigned to peaks at 1600 cm^{-1}, 1513 cm^{-1}, and 1425 cm^{-1}. The magnified region of FT-IR spectra indicated that syringyl- (S-) and guaiacyl-type (G-type) lignins existed in all lignin fractions (Tian et al., 2015). However, the signal intensity of S- and G-type subunits in L_O and

Table 1
The chemical composition and content (wt% dry lignin) of alkaline DES-extracted lignin (L_O) and its acid precipitated three lignin fractions (L_6, L_4, and L_2).

	DES lignin samples			
	L_O	L_6	L_4	L_2
AIL	73.29 ± 2.01	78.58 ± 0.69	88.26 ± 1.58	91.37 ± 0.39
ASL	1.81 ± 0.10	0.48 ± 0.05	1.38 ± 0.26	1.53 ± 0.13
Ash[a]	15.01 ± 0.41	61.62 ± 0.59	4.27 ± 0.41	2.21 ± 0.25
Lignin purity[b]	60.09	17.44	85.37	90.69
Lignin yield[c]	7.83	4.54	2.07	1.19
Glucose	0.65 ± 0.01	0.24 ± 0.00	0.36 ± 0.01	0.37 ± 0.00
Xylose	1.14 ± 0.02	0.27 ± 0.00	1.13 ± 0.01	1.34 ± 0.01
Arabinose	0.67 ± 0.01	0.25 ± 0.00	0.85 ± 0.03	0.86 ± 0.00
Galactose	0.52 ± 0.01	0.18 ± 0.00	0.34 ± 0.01	0.31 ± 0.00
Mannose	0.10 ± 0.00	< 0.1	< 0.1	< 0.1
Rhamnose	< 0.1	< 0.1	0.13 ± 0.01	0.13 ± 0.00
Carbohydrates[d]	3.30	1.24	3.01	3.20
Polysaccharides[e]	2.91	1.11	2.67	2.84

[a] The total amount of ash in raw lignin samples was determined gravimetrically based on the standardized technical report (NREL) (Sluiter et al., 2008).
[b] Lignin purity was calculated from the formula of AIL (wt%) + ASL (wt%)–Ash (wt%).
[c] Yields of lignin samples were based on the dry weight of wheat straw (obtained lignin/original biomass, w/w).
[d] Sum of monosaccharides.
[e] The polysaccharide content was calculated from the corresponding monosaccharides using an anhydro correction: pentoses (wt%) × 0.88 + hexoses (wt %) × 0.9 (Willför et al., 2009).

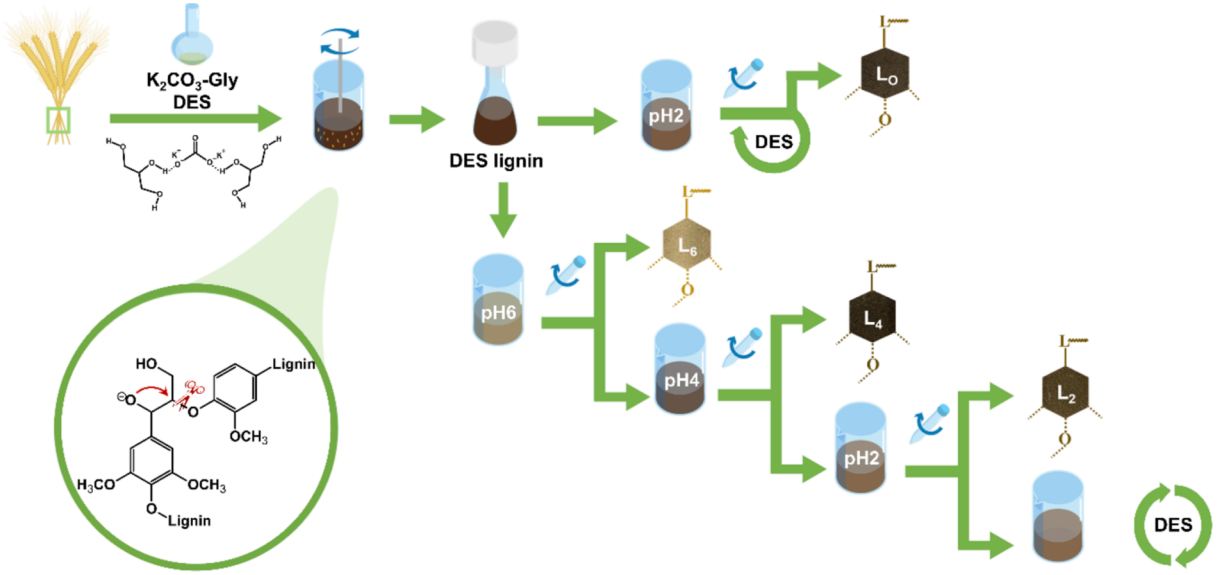

Fig. 1. Experimental procedure for fractionation of lignin from wheat straw with alkaline DES extraction and sequential acid fractionation.

L_6 is relatively weak due to the strong interference from impurities. In addition, the bands at 1091 cm^{-1} and 800 cm^{-1} were attributed to the stretching vibrations of Si − O − Si, and the signal at 467 cm^{-1} was due to Si − O bending vibrations, which were recorded in L_O and L_6 while being almost fully absent with L_4 and L_2 (Bula et al., 2015). These strong signals particularly with L_6 originated likely from the plentiful ash content.

3.2. Elemental composition of lignin fractions

All the lignin samples displayed a typical elemental composition attributed with the lignin backbone structure (Table 2), and the content of individual elements was also found to be precisely similar to previously published data (Zhao et al., 2020). However, L_6 fraction had substantially lower content of all these elements, and it was rich in Si, while only extremely small amounts of Si were detected in L_4 and L_2 fractions (Table 1). Moreover, the unfractionated DES lignin L_O contained a notable amount of Si, which is in line with the high ash content of these samples. The C content was also in accordance with lignin purity results.

The ratio of the atomic concentrations of oxygen and carbon (O/C) was found to be lower with L_4 and L_2 fractions (~0.36), which was close to the theoretical O/C value of lignin (0.33) (Wei et al., 2018), thus revealing the high lignin concentration as corroborated also by purity results. The high O/C ratio in L_O and L_6 fractions in turn reflected the high proportion of oxygen-containing silicates (SiO_2).

The quantitative XPS is to further interpret the linkage bonds of lignins (see supplementary material). The comparison between L_4 and L_2 revealed that the lignin fractions precipitated at lower pH possessed lower C2 and higher C3 contents (Fig. 2(h)), corresponding to lower O3 and higher O2 contents (Fig. 2(l)), alluding the increase in C = O subunits. The disappearance of the C3 peak in L_6 in turn indicated a low C = O amount, which was further evidenced by the FT-IR pattern. These changes in C–O and C = O linkages implied that the precipitation of oxidized lignin occurred at a low pH condition and were subsequently confirmed with the FT-IR, ^{13}C NMR, and 2D-NMR analysis.

3.3. Molecular weight and thermal stability of lignin fractions

The acid-precipitated lignin fractions displayed significant differences in their weight-average (Mw) and number-average molecular weights (Mn) (Fig. 3(a)). As the acidity of the precipitation system increased, Mw decreased from 4036 to 2811 g/mol and Mn decreased from 1057 to 952 g/mol, from which it can be deduced that the lignin fractions with a large molecular size precipitated already under slightly acidic conditions, whereas lignin fractions with small molecular weight required stronger acidic conditions for precipitation. It has been reported that lignin with a low molecular weight contains typically more hydrophilic groups (such as hydroxyl (Ar − OH) and carboxyl (−COOH) groups) (Ma et al., 2020), requiring a higher acid concentration to reduce the degree of ionization and cause lignin deposition. In all fractions, L_2 fraction had the narrowest molecular weight distribution (PDI of 2.95), indicating a high level of homogeneity of molecular weight in the lignin fraction precipitated at low pH condition. A comparison with L_O shows that sequential acid precipitation is notably beneficial in obtaining lignin with a relatively narrowly distributed and small molecular weight. Overall, the L_2 fraction had lower Mw and Mn than previously reported with milled wood lignin (MWL), alkaline lignin, and acetic acid lignin (see supplementary material) (Pan and Sano, 2000). This indicates that lignin fraction with low molecular weight can be separated from alkaline DES lignin filtrate by a simple and continuous acid precipitation process.

The thermal properties of lignin fractions were revealed by thermogravimetric (TGA) and differential thermogravimetric (DTG) analysis (Fig. 3(b-c)). The details of thermal characteristics of lignins in terms of decomposition temperature (T_M) and the maximum degradation rate (V_M) are presented thoroughly (see supplementary material). All the lignin samples displayed a broad, three-stage TGA decomposition curve in agreement with previous literatures (Pang et al., 2020), however, the thermal stability of L_6 was visibly different from the other three lignin fractions. The notable residue amount of L_6 was ascribed its conspicuous silicate content (ash) as also indicated by the purity analysis. It is also the primary cause of the low V_M of L_6.

Table 2
Elemental composition of DES lignin fractions determined by elemental (% dry lignin, w/w), XPS (atomic %), and XRF (% dry lignin, w/w) analysis.

Element		L_O	L_6	L_4	L_2
C	Elemental	50.20 ± 0.49	20.16 ± 0.44	60.21 ± 0.10	61.06 ± 0.11
	XPS	62.47	30.54	72.08	72.42
H	Elemental	5.70 ± 0.08	2.55 ± 0.08	5.61 ± 0.06	5.70 ± 0.03
	XPS	–	–	–	–
O	Elemental	22.60 ± 0.39	11.31 ± 0.50	28.18 ± 0.07	28.86 ± 0.20
	XPS	28.75	48.16	25.77	25.99
N	Elemental	1.10 ± 0.01	0.36 ± 0.02	1.32 ± 0.01	1.22 ± 0.00
	XPS	–	0.88	1.92	1.81
S	Elemental	<0.10	–	–	–
	XPS	–	–	–	–
Si	Elemental	–	–	–	–
	XPS	7.59	19.98	–	–
	XRF	8.65	27.32	2.21	1.90
O/C	Elemental	–	–	–	–
	XPS	0.46	1.57	0.36	0.36

3.4. DES lignin nanospheres: The visual appearance and particle size

The alkaline DES-isolated lignin (L_O) and its three fractions (L_6, L_4, and L_2) were further exploited to fabricate solid spherical nanospheres via solvent-exchange approach. The appearance of dry and highly concentrated LNPs as revealed by FESEM (see supplementary material). All the samples contained spherical nanoentities in a wide, submicron size range, being tightly aggregated together. The TEM images further illustrate the individual nanoparticles in a dispersed and low-concentration medium and the color of lignin fractions also varied considerably (see supplementary material), with L_4 being the darkest, probably is related to the larger S/G ratio (the content ratios of syringyl to guaiacyl units), namely, high content of methoxy groups, which is in accordance with previous research (Zhang et al., 2019). Besides, functional groups in lignin, such as α-carbonyl, biphenyl, and ring-conjugated double bonds, may have contributed to the coloration (Pan et al., 2022). In contrast, the lighter color of L_6 was mainly caused by the presence of a large amount of whitish silica.

The formation mechanism of lignin nanospheres was ascribed to the entry of DIW into lignin-THF solution system, which altered the hydrophobicity–hydrophilicity balance during the solvent shifting process. The hydrophilic groups (e.g., −OH and − COOH functional groups) of the lignin skeleton extended outwards in the aqueous environment to form outside layers of particles. On the other hand, the hydrophobic chain segments (phenylpropane structures, etc.) protruded inwards to create solid spheres (Pang et al., 2020). Therefore, we propose a hypothesis, as shown in Fig. 4 regarding the formation mechanism of lignin macromolecular aggregations and LNPs formation resulting from different content of hydrophilic groups. In general, hydrophobic interactions, hydrogen bonding, π-interactions, and van der Waals forces drive the macromolecular coordination of lignin molecules into nanospheres during the self-assembly process (Xiong et al., 2017).

The size distribution of lignin nanospheres (Fig. 3(g–j)), as determined by the image analysis of electron microscopy images using ImageJ software, was 200–400 nm (~79%), 300–400 nm (~70%), 400–500 nm (~75%), and 600–700 nm (~78%) for LNP_O, LNP_6, LNP_4,

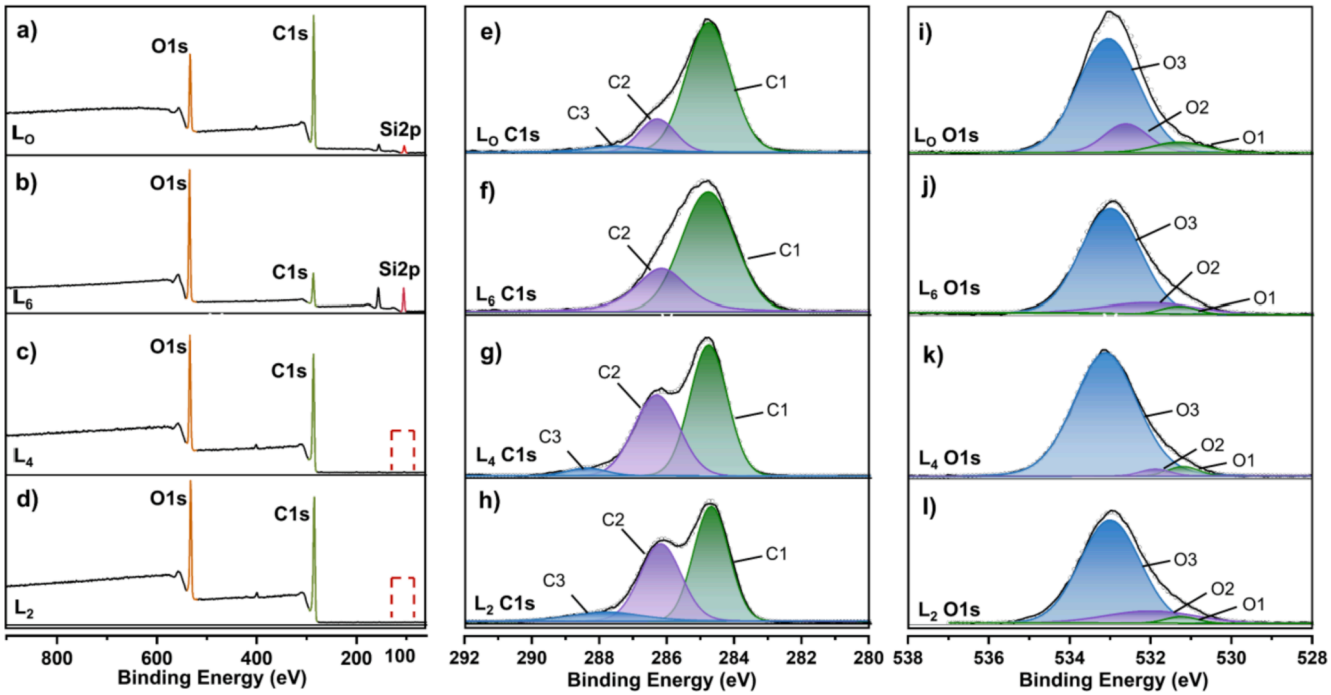

Fig. 2. The survey XPS spectra of lignin fractions (a-d); The curve fitting of C1s and O1s XPS spectra of DES lignin fractions: (e) and (i) L_O, (f) and (j) L_6, (g) and (k) L_4, and (h) and (l) L_2. (The C1 atoms are linked to carbon (C − C) and hydrogen (C − H) groups, assigned to the aliphatic and aromatic carbons of lignin; the C2 atoms are bonded to non-carbonyl oxygen atoms (C − O) and can be generically categorized as phenolic and ether molecules; the C3 atoms are linked with carbonyl oxygen atoms (C = O) attributed to carbonyl groups in lignin. The O 1 s spectra originate from O1 atoms associated with Ph = O, Ph − C = O, and O–O components; the O2 atoms are bonded to carbon with a double bond (O–C = O); the O3 is in turn related to carbon with a single bond (C–O–)).

and LNP_2, respectively, with LNP_2 consisting of the most uniform and well-shaped particles. Additionally, LNP_6 has a different morphology compared with other nanosphere fractions, and it contained a significant portion of irregular coprecipitates in which the LNPs were encapsulated. These coprecipitates were likely caused by the high presence of silicates in L_6 fraction. Consequently, all the LNPs in L_6 were not clearly visible as individual particles, and their size was difficult to determine.

The LNPs possessed different negative zeta potential (~from − 38 mV to − 51 mV) (Fig. 3(d)). Lignin macromolecules extracted by alkaline DES (pH≈12) were dissolved in alkaline solution to form a stable system as illustrated in Fig. 4. When the alkaline DES lignin solution changed to acid, the H^+ neutralized the negative charge on lignin surface and disrupted the balance of original system. Some lignin macromolecules carrying low amount of Ar − OH and − COOH groups reached saturation firstly at low H^+ concentration and preferentially aggregated and precipitated out. With the increase of H^+ concentration, different lignin fractions were separated sequentially under various pH value.

The average particle diameters of LNPs obtained from DLS increased in the order of L_6 (323.71 nm) < L_O (370.26 nm) < L_4 (457.43 nm) < L_2 (653.90), being in line with the results of image analysis. Apparently, the L_2 fraction had the highest surface charge density (zeta potential), resulted in the formation of largest nanospheres, which may have been caused by electrostatic repulsion between the charged lignin domains. And this favored more open molecular packing in the LNPs. Moreover, the hydrophilic nature of charged lignin moieties likely enhanced the interaction of lignin with water in the solvent shifting system, leading to the formation of larger nanospheres (Liu et al., 2019). Here, in order to evaluate the stability of DES lignin nanospheres, the average diameter and zeta potential over a period of 90 days were measured (Fig. 3(e-f)). No significant changes were observed in the average diameter and zeta potential, indicating that these nanospheres stayed highly stable.

3.5. Nuclear magnetic resonance analysis of lignin fractions

3.5.1. ^{13}C NMR and ^{31}P NMR

The overall structure of lignin macromolecule and lignin carbon skeleton was elucidated from acetylated lignin samples with quantitative ^{13}C NMR spectra (see supplementary material). The integral of the aromatic region (160–103 ppm) was set as the reference for quantification. Subsequently, the other regions of the spectrum were also analyzed to obtain the number of substituents per aromatic ring (Ar). Table 3 lists and interprets the detailed data based on previous studies (Holtman et al., 2004; Wen et al., 2013).

The resonance of − CH_3 in the acetyl group appeared abruptly at 21 ppm in all of lignin fractions. The data showed three resonance regions at 80.2, 74.0, and 62.1 ppm, attributed to β − O − 4 subunit linked with C − β, C − α, and C − γ, respectively, indicating that residual β − O − 4 bonds existed in the isolated lignin at different levels in the order of L_2 < L_4 < L_O < L_6. The strong resonance at 55.8 ppm was attributed to the − OCH_3 group in the S and G units in different contents in the order of L_2 < L_4 < L_O < L_6. The amount of − OH groups was measured from 171 to 166 ppm of acetylated lignin samples, with the signals at 171–169.6 ppm, 169.6–168.6 ppm, and 168.6–166 ppm being defined as primary − OH, secondary − OH, and Ar − OH groups, respectively. The total − OH content was in the order of L_2 > L_4 > L_O > L_6, in opposite sequence to that of the residual β − O − 4 bonds and − OCH_3 groups. The results showed that the − OH content of lignin was related to its residual β − O − 4 bonds and the content of S and G units. The results of the content of − OH groups were in accordance with that of ^{31}P NMR results showed in Table 3. Moreover, the increase in Ar − OH content as a function of acidity of precipitation was in line with the aggregation behavior of lignin fractions.

The deconvoluted quantitative ^{31}P NMR spectra were applied to interpret the hydroxyl characteristics of lignin (see supplementary material). The spectra were scaled so that the peak heights of the IS were approximately the same. The automatic fitting algorithm was used to

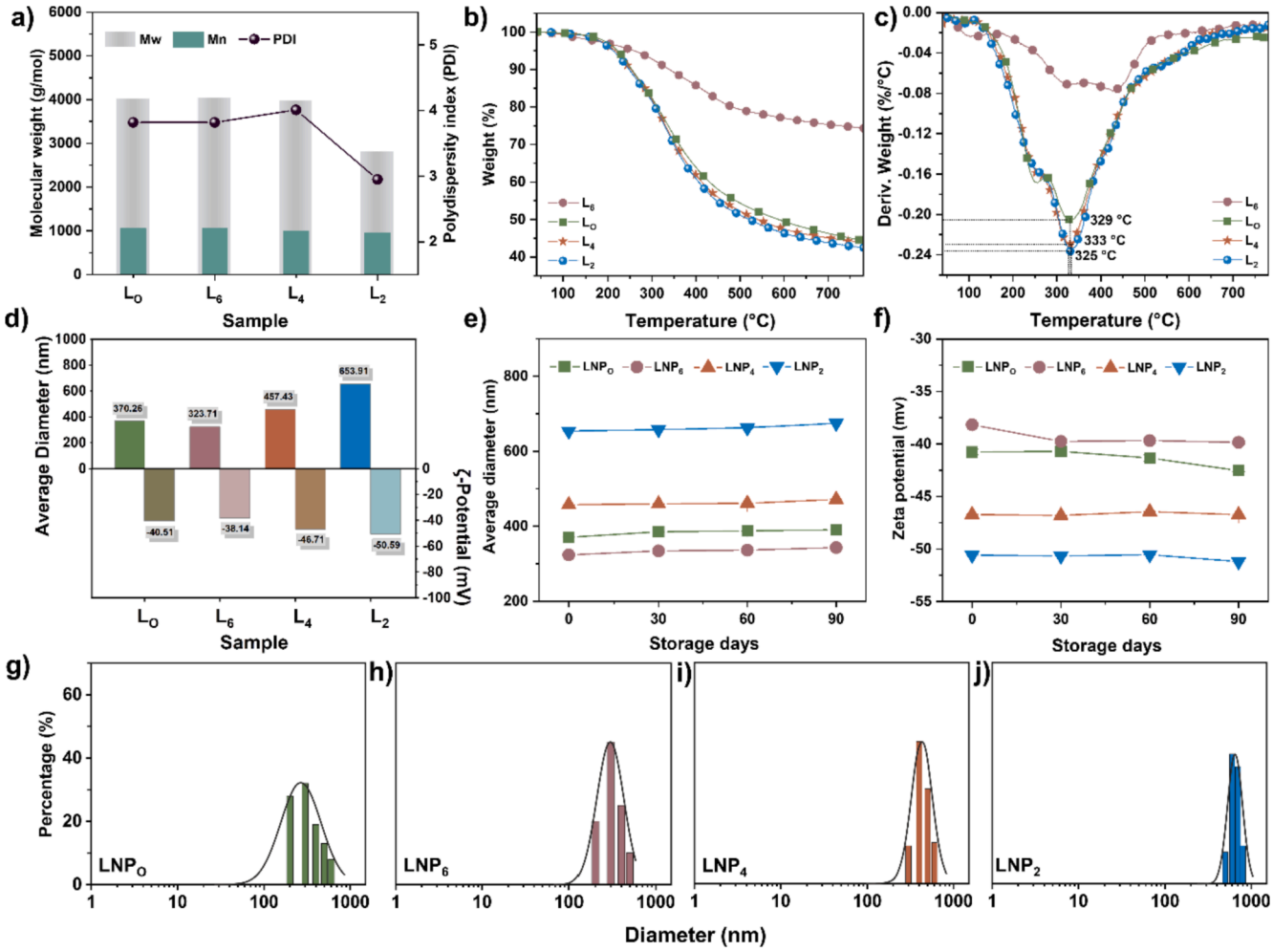

Fig. 3. (a) The molecular weight and polydispersity index of DES lignin fractions, (b-c) TG and DTG curves of lignin fractions, (d) Zeta potential and particle size of lignin nanospheres measured by DLS in deionized water, (e-f) Stability of DES lignin nanospheres: variations of (e) average diameter and (f) zeta potential of nanospheres in deionized water as a function of time, (g-j) size distributions of lignin nanospheres.

deconvolute the spectral region and optimize the number of peaks according to the best fit (OriginPro 2020b, Northampton, MA, USA). Table 3 presents the quantitative values of each spectral integration region.

Among the many signals of − OH groups, the aliphatic − OH signal was regularly the dominant in lignins. Moreover, it was also noted that the Ar − OH functional groups were primarily derived from syringyl and guaiacyl OH. The predominance of syringyl and guaiacyl units, along with the presence of *p*-hydroxyphenyl, confirms that lignins in this study are the typical grass lignins (Grabber et al., 2004). Furthermore, different lignin fractions had significantly different Ar − OH and − COOH contents (Table 3). The total Ar − OH content increased with the decrease of the fractionation pH, with the total Ar − OH content of L_2 fraction being the highest (9.60 mmol/g). Besides, the content of − COOH decreased in the order of $L_2 > L_4 > L_O > L_6$ (Fig. 5(c)). Overall, the Ar − OH content of L_4 and L_2 was considerably higher than the values reported in literature (see supplementary material) (Crestini and Argyropoulos, 1997; Zikeli et al., 2016).

Ar − OHs and − COOHs are the key functional groups in lignin, and they contribute to its hydrophilicity and further utilization in lignin composites. Therefore, the combined DES extraction and sequential acid fractionation is a promising approach to obtain lignin with a high proportion of reactive and hydrophilic functional groups. However, the high hydrophilic group content was not conducive to form lignin nanospheres due to the ionization of − OH and − COOH groups and the hydrogen bonding between lignin and water. In particular, the increase of Ar − OH in L_2 leads to the strengthening of the hydrogen bond interactions between lignin and water, hindering the self-assembly of lignin macromolecules (Zhao et al., 2017). Moreover, the electrostatic repulsion caused by ionized Ar − OHs of lignin precluded the regeneration of nanospheres with a condensed core (Zhao et al., 2017). However, when lignin with a higher content of Ar − OH and − COOH forms nanoparticles, the hydrogen bonds between lignin and water are transformed into intermolecular hydrogen bonds of lignin, and larger lignin particles will be formed. This conclusion was consistent with the visual appearance (see supplementary material) and particle size of lignin nanospheres (Fig. 3(g-j)).

3.5.2. 2D HSQC-NMR

2D HSQC-NMR was performed to provide more detailed information about the linkages and aromatic structure of lignins. All the lignin samples had similar types of subunits, but their overall contents differed (Fig. 5 (a)). The aliphatic regions (δC/δH 40–90/2.5–5.8 ppm) are displayed in the left column. The signals of − OCH_3 on the aromatic ring (δC/δH 56.2/3.74 ppm) were the most notable in this region. The abundant − OCH_3 groups attributed to S- and G-type units enhanced the electronic interactions between lignin molecules in aqueous media, which is an important factor that affects the aggregation behavior of lignin. The aromatic regions (δC/δH 100–140/6.0–8.0 ppm) shown in the right column present the contents of aromatic units and S/G ratios.

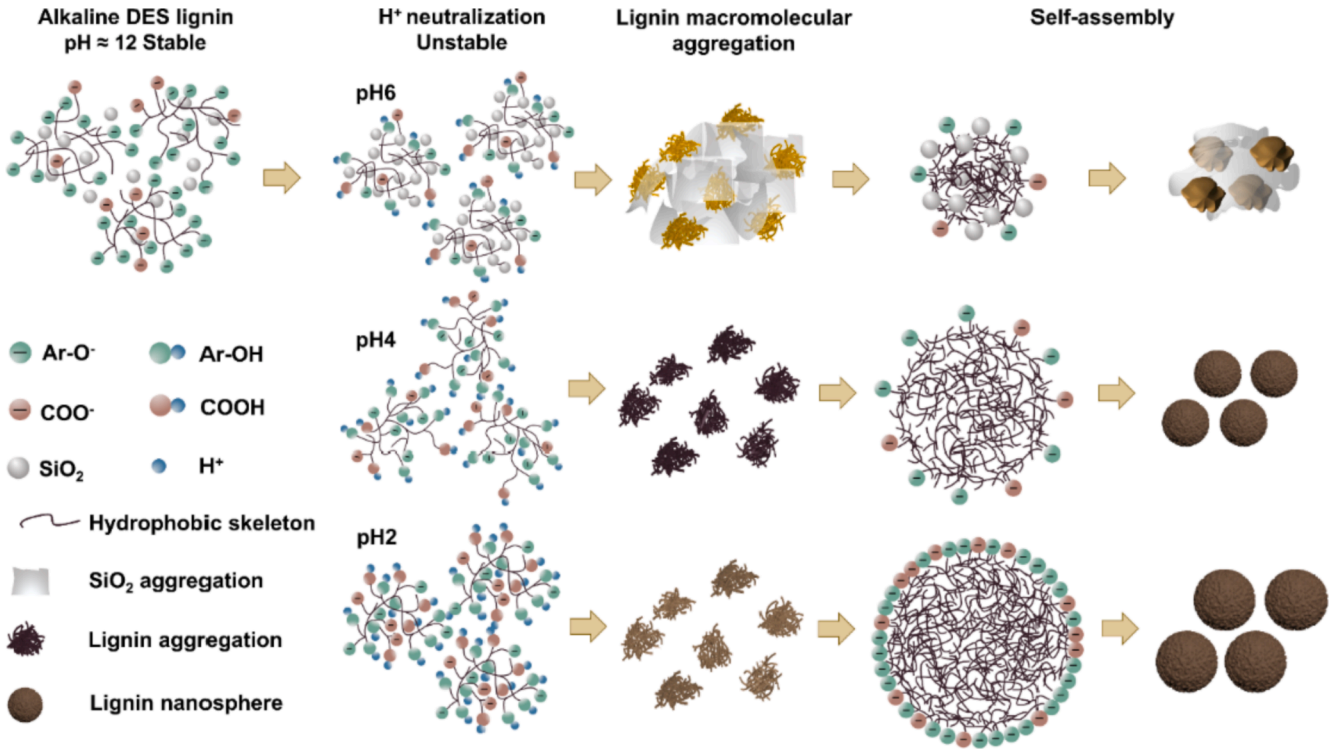

Fig. 4. Proposed schematic for the mechanism of lignin macromolecular aggregation and lignin nanospheres formation resulting from different lignin fractions.

Table 3
Quantitative ^{13}C NMR and ^{31}P NMR analysis of the lignin fractions.

NMR spectra	Spectral region	Chemical shift (ppm)	Content[a]			
			L_O	L_6	L_4	L_2
^{13}C NMR	CH_3O	57–54	1.62	1.94	1.55	1.38
	CAr − H	125–100	2.04	1.67	1.95	1.77
	CAr − C	141–125	2.17	1.57	1.44	1.51
	CAr − O	160–141	1.79	2.76	2.95	2.73
	Primary − OH	171–169.6	0.12	0.04	0.37	0.51
	Secondary − OH	169.6–168.6	0.04	0.05	0.12	0.19
	Phenolic − OH	168.6–166	0.10	0.02	0.28	0.57
	$-CH_3$ and $-CH_2$ in aliphatic side chain	34–12	3.09	2.97	3.01	2.88
	C_γ in $\beta-O-4$ with C = O	64–61	0.45	0.28	0.13	0.22
	C_α in $\beta-O-4$	77–71	0.61	0.66	0.53	0.50
	C_β in $\beta-O-4$	83–77	0.59	0.64	0.57	0.51
^{31}P NMR	Aliphatic − OH	149.0–144.7	2.00	0.75	6.63	11.25
	Syringyl − OH (S-units)	142.8–140.6	0.54	0.20	1.89	3.60
	C_5 substituted and guaiacyl − OH (5-sub. and G-units)	140.5–137.5	0.84	0.37	2.39	4.69
	p-Hydroxyphenyl − OH (H-units)	137.5–136.0	0.19	0.03	0.60	1.31
	Tricin	136.0–134.7	0.11	0.02	0.12	0.67
	Carboxylic − OH	134.7–132.7	0.46	0.08	0.73	2.52
	Total phenolic − OH[b]	142.8–136.0	1.57	0.60	4.88	9.60

[a] Units: ^{13}C NMR: moieties per Ar; ^{31}P NMR: mmol/g lignin.
[b] Total content of phenolic − OH group (i.e., guaiacyl, syringyl, C_5-substituted guaiacyl phenolics, *p*-hydroxyphenols).

The detailed information of lignin substructures was assigned based on previous research data (Domínguez-Robles et al., 2017; Yuan et al., 2011; Zikeli et al., 2016).

As the acidity in lignin precipitation increased, the proportions of β–O–4 linkages in lignin fractions decreased significantly, while the percentage of β–5 and β-β linkages increased (Fig. 5 (b)). As illustrated by ^{31}P NMR analysis, the lignin deposited under a lower pH had more Ar − OH and − COOH groups, and the cleavage of β–aryl ether bonds was presumably the main factor in the production of Ar − OHs. The syringyl (S) and guaiacyl (G) units accounted for high percentage in all the lignin fractions as shown by the integral quantification from aromatic regions (Fig. 5 (b)). The S/G ratio declined for the three fractions ($L_6 > L_4 > L_2$) which might be because the lignin fractions with high G (G + G') units contained more β–5 linkages, while the lignin fraction with high S (S + S') units contained more β–O–4 and β–β structures, which was consistent with the information of 2D-NMR spectra in aliphatic part. Previously, the aggregation of lignin molecules was found to be influenced by noncovalent π–π interactions between different aromatic units, and this effect decrease in the order of S > G > H subunits (Ma et al., 2020). The stronger π–π stacking interactions were conducive to tighten bounds of lignin molecules, thus forming nanospheres with a dense structure during the self-assembly process. However, the content of hydrophilic groups was likely the primary factor that affects the formation of lignin nanospheres.

3.6. Potential mechanism for alkaline DES-extracted lignin fractions from wheat straw

The information of structure and characteristics of different lignin fractions provides penetrating insights into the potential mechanism involved in lignin extraction by alkaline DES from wheat straw. Furthermore, 2-(2-methoxyphenoxy)-1-(3,4-dimethoxyphenyl)propane-1,3-diol (VG), a β–O–4 linked lignin dimer, was harnessed as a model compound in alkaline DES under 95 °C to reveal the lignin reaction mechanisms in DES medium. VG was found to be completely converted in DES, resulting in almost stoichiometric production of guaiacol, and several products with ketone side chain were identified. These results were similar to the degradation of lignin models under alkaline cooking conditions, although it is difficult to determine the detailed mechanism due to the complexity of the reaction (Kato et al., 2019). This at least indicates that the cleavage of ether bonds is one of the main reaction routes causing the lignin depolymerization and

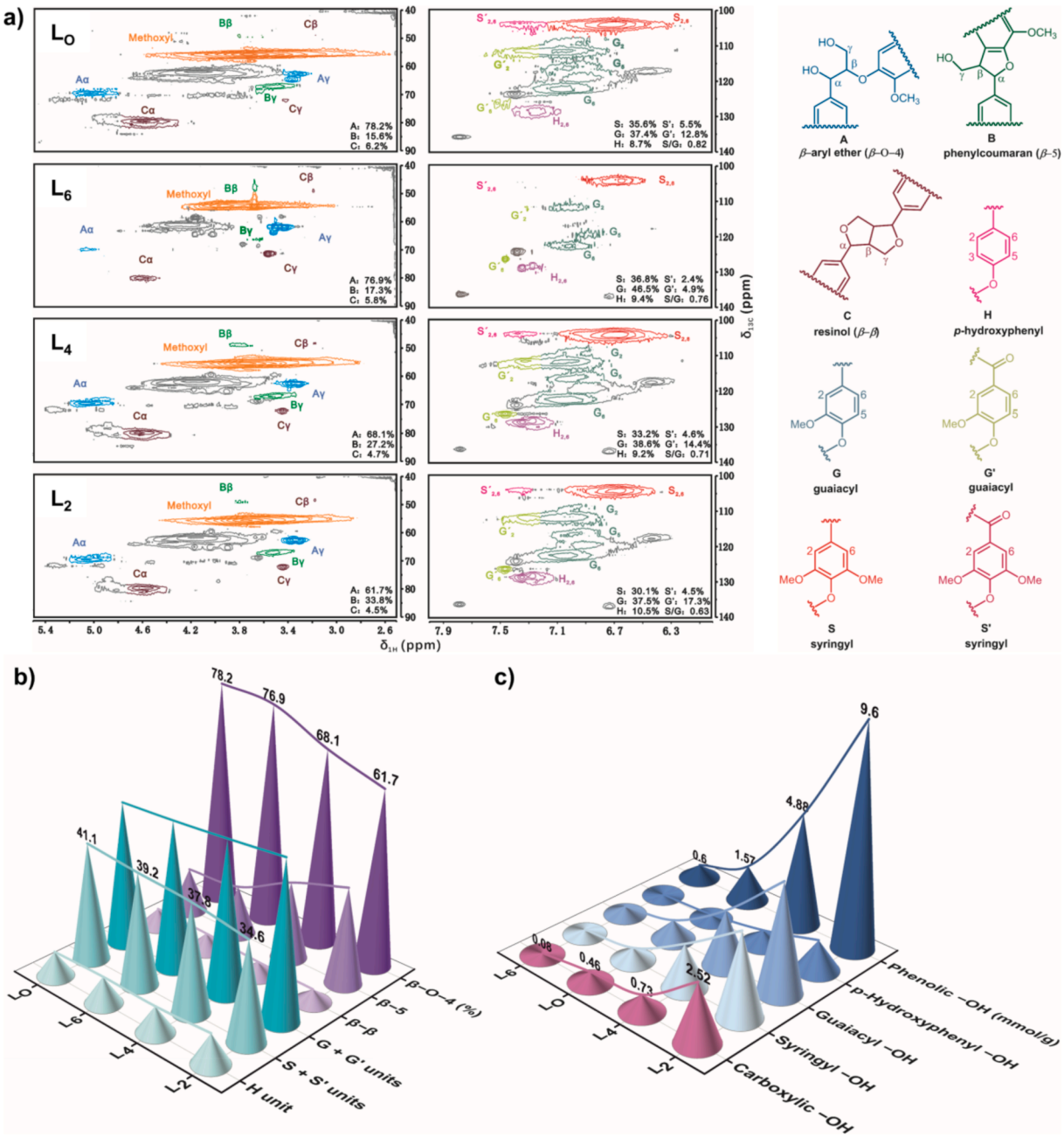

Fig. 5. (a) 2D HSQC-NMR spectra of DES lignin fractions: (A) *β*–aryl ether (*β*–O–4); (B) phenylcoumaran (*β*–5); (C) resinol (*β*–*β*) linkages; (H) *p*-hydroxyphenyl; (G) guaiacyl; (G') oxidized guaiacyl; (S) syringyl; (S') oxidized syringyl. (b) Comparison of major interunit linkage and subunit contents in different lignin fractions from 2D HSQC-NMR quantitative analysis. (c) hydroxyl contents of DES lignin fractions measured by ^{31}P NMR.

facilitating lignin extraction from wheat straw (see supplementary material).

There are limitations in applying the existing knowledge to understand the reactivity of lignin degradation under alkaline conditions, because the lignin models, reaction conditions, and methods for quantification vary in the literature. In addition, the complex further reactions of epoxide side chain intermediates of lignin degradation are the main reason for revealing the degradation mechanism of lignin under alkaline conditions. Although the further reactions of the epoxide side chain intermediates are quite complicated, the data of 2D-NMR showed that oxidized (Cα = O) guaiacyl units G' and syringyl units S' were the main structure of products, which are commonly found in alkaline lignin (Mancera et al., 2011). To conclude, based on the available evidence, the lignin degradation reaction mechanism in alkaline DES treatment is similar to that in NaOH pulping (Kato et al., 2019). This mechanism results in lignin with a high − OH and − COOH content, which can be a benefit in developing a wider range of lignin applications.

4. Conclusions

The lignin fraction with high purity and plentiful hydroxyl and carboxyl groups was fractionated by sequential, three-step, acidic precipitation method. The *β* aryl ether bond cleavage is a primary route to facilitate lignin extraction from wheat straw via alkaline DES treatment, similar to traditional NaOH pulping. The hydrophilic functional groups as well as purity are essential for the formation of controllable morphological lignin nanospheres. The findings related to the dissociation mechanism and fractionation of reactive lignin during alkaline

DES pretreatment and the acid sequence precipitation are crucial for facilitating lignin valorization in high-added value products.

CRediT authorship contribution statement

Xin Yue: Investigation, Methodology, Formal analysis, Data curation, Writing – original draft. **Terhi Suopajärvi:** Resources, Supervision, Writing – review & editing. **Shirong Sun:** Formal analysis, Writing – review & editing. **Otto Mankinen:** Software, Data curation, Writing – review & editing. **Atte Mikkelson:** Data curation. **Harri Huttunen:** Data curation. **Sanna Komulainen:** Data curation. **Idamaria Romakkaniemi:** Data curation. **Juha Ahola:** Data curation, Writing – review & editing. **Ville-Veikko Telkki:** Data curation, Writing – review & editing. **Henrikki Liimatainen:** Conceptualization, Supervision, Writing – review & editing.

Declaration of Competing Interest

The authors declare that they have no known competing financial interests or personal relationships that could have appeared to influence the work reported in this paper.

Data availability

Data will be made available on request.

Acknowledgments

The financial support of China Scholarship Council (CSC), the Regional Council of Kainuu, the funding granted by the European Regional Development Fund of the European Union for TELI project, and Tauno Tönning Foundation grants are gratefully acknowledged. We also would like to thank the support of Center of Microscopy and Nanotechnology in the University of Oulu and Jasmiini Tornberg for revising the experimental procedure diagram.

Appendix A. Supplementary data

Supplementary data to this article can be found online at https://doi.org/10.1016/j.biortech.2022.127570.

References

Brandt, A., Chen, L., van Dongen, B.E., Welton, T., Hallett, J.P., 2015. Structural changes in lignins isolated using an acidic ionic liquid water mixture. Green Chem. 17 (11), 5019–5034.
Bula, K., Klapiszewski, Ł., Jesionowski, T., 2015. A novel functional silica/lignin hybrid material as a potential bio-based polypropylene filler. Polym. Compos. 36 (5), 913–922.
Chen, Z., Ragauskas, A., Wan, C., 2020. Lignin extraction and upgrading using deep eutectic solvents. Ind. Crops Prod. 147, 112241.
Crestini, C., Argyropoulos, D.S., 1997. Structural analysis of wheat straw lignin by quantitative 31P and 2D NMR spectroscopy. The occurrence of ester bonds and α-O-4 substructures. J. Agric. Food. Chem. 45 (4), 1212–1219.
Deniz, I., Kırcı, H., Ates, S., 2004. Optimisation of wheat straw Triticum drum kraft pulping. Ind. Crops Prod. 19 (3), 237–243.
Domínguez-Robles, J., Sánchez, R., Espinosa, E., Savy, D., Mazzei, P., Piccolo, A., Rodríguez, A., 2017. Isolation and characterization of gramineae and fabaceae soda lignins. Int. J. Mol. Sci. 18 (2), 327.
Grabber, J.H., Ralph, J., Lapierre, C., Barrière, Y., 2004. Genetic and molecular basis of grass cell-wall degradability. I. Lignin–cell wall matrix interactions. C.R. Biol. 327 (5), 455–465.
Holtman, K.M., Chang, H.-M., Kadla, J.F., 2004. Solution-state nuclear magnetic resonance study of the similarities between milled wood lignin and cellulolytic enzyme lignin. J. Agric. Food. Chem. 52 (4), 720–726.
Huijgen, W., Telysheva, G., Arshanitsa, A., Gosselink, R., De Wild, P., 2014. Characteristics of wheat straw lignins from ethanol-based organosolv treatment. Ind. Crops Prod. 59, 85–95.
Jasiukaitytė-Grojzdek, E., Kunaver, M., Crestini, C., 2012. Lignin Structural Changes During Liquefaction in Acidified Ethylene Glycol. J. Wood Chem. Technol. 32 (4), 342–360.
Ji, H., Lv, P., 2020. Mechanistic insights into the lignin dissolution behaviors of a recyclable acid hydrotrope, deep eutectic solvent (DES), and ionic liquid (IL). Green Chem. 22 (4), 1378–1387.
Kato, Y., Shimizu, S., Akiyama, T., Yokoyama, T., Matsumoto, Y., 2019. Effect of Counter Cation on Alkaline Reaction of β-O-4-Type Substructure in Lignin. J. Wood Chem. Technol. 39 (2), 111–123.
Lim, W.-L., Gunny, A.A.N., Kasim, F.H., AlNashef, I.M., Arbain, D., 2019. Alkaline deep eutectic solvent: a novel green solvent for lignocellulose pulping. Cellulose 26 (6), 4085–4098.
Liu, Z.-H., Hao, N., Shinde, S., Pu, Y., Kang, X., Ragauskas, A.J., Yuan, J.S., 2019. Defining lignin nanoparticle properties through tailored lignin reactivity by sequential organosolv fragmentation approach (SOFA). Green Chem. 21 (2), 245–260.
Lou, R., Zhang, X., 2022. Evaluation of pretreatment effect on lignin extraction from wheat straw by deep eutectic solvent. Bioresour. Technol. 344, 126174.
Ma, M., Dai, L., Xu, J., Liu, Z., Ni, Y., 2020. A simple and effective approach to fabricate lignin nanoparticles with tunable sizes based on lignin fractionation. Green Chem. 22 (6), 2011–2017.
Mancera, C., Ferrando, F., Salvadó, J., El Mansouri, N.E., 2011. Kraft lignin behavior during reaction in an alkaline medium. Biomass Bioenergy 35 (5), 2072–2079.
Pan, X.-J., Sano, Y., 2000. Comparison of acetic acid lignin with milled wood and alkaline lignins from wheat straw. Holzforschung 54 (1), 61–65.
Pan, Z., Li, Y., Zhang, Z., Xu, F., Ramaswamy, S., Abdulkhani, A., Zhang, X., 2022. Fractionation of light-colored lignin via lignin-first strategy and enhancement of cellulose saccharification towards biomass valorization. Ind. Crops Prod. 186, 115173.
Pang, T., Wang, G., Sun, H., Wang, L., Liu, Q., Sui, W., Parvez, A.M., Si, C., 2020. Lignin fractionation for reduced heterogeneity in self-assembly nanosizing: toward targeted preparation of uniform lignin nanoparticles with small size. ACS Sustain. Chem. Eng. 8 (24), 9174–9183.
Sethupathy, S., Morales, G.M., Gao, L., Wang, H., Yang, B., Jiang, J., Sun, J., Zhu, D., 2022. Lignin valorization: Status, challenges and opportunities. Bioresour. Technol. 126696.
Shen, X.-J., Chen, T., Wang, H.-M., Mei, Q., Yue, F., Sun, S., Wen, J.-L., Yuan, T.-Q., Sun, R.-C., 2020. Structural and Morphological Transformations of Lignin Macromolecules during Bio-Based Deep Eutectic Solvent (DES) Pretreatment. ACS Sustain. Chem. Eng. 8 (5), 2130–2137.
Shuai, L., Amiri, M.T., Questell-Santiago, Y.M., Héroguel, F., Li, Y., Kim, H., Meilan, R., Chapple, C., Ralph, J., Luterbacher, J.S., 2016. Formaldehyde stabilization facilitates lignin monomer production during biomass depolymerization. Science 354 (6310), 329–333.
Sluiter, A., Hames, B., Ruiz, R., Scarlata, C., Sluiter, J., Templeton, D., Crocker, D. 2008. Determination of structural carbohydrates and lignin in biomass US National Renewable Energy Laboratory. NREL/TP-510-42618.
Suopajärvi, T., Ricci, P., Karvonen, V., Ottolina, G., Liimatainen, H., 2020. Acidic and alkaline deep eutectic solvents in delignification and nanofibrillation of corn stalk, wheat straw, and rapeseed stem residues. Ind. Crops Prod. 145, 111956.
Tian, Z., Zong, L., Niu, R., Wang, X., Li, Y., Ai, S., 2015. Recovery and characterization of lignin from alkaline straw pulping black liquor: As feedstock for bio-oil research. J. Appl. Polym. Sci. 132 (25), 42057.
Wei, Y., Huang, Y., Yu, Y., Gao, R., Yu, W., 2018. The surface chemical constituent analysis of poplar fibrosis veneers during heat treatment. Journal of Wood Science 64 (5), 485–500.
Wen, J.-L., Sun, S.-L., Xue, B.-L., Sun, R.-C., 2013. Quantitative structural characterization of the lignins from the stem and pith of bamboo (Phyllostachys pubescens). Holzforschung 67 (6), 613–627.
Willför, S., Pranovich, A., Tamminen, T., Puls, J., Laine, C., Suurnäkki, A., Saake, B., Uotila, K., Simolin, H., Hemming, J., 2009. Carbohydrate analysis of plant materials with uronic acid-containing polysaccharides–A comparison between different hydrolysis and subsequent chromatographic analytical techniques. Ind. Crops Prod. 29 (2–3), 571–580.
Xiong, F., Han, Y., Wang, S., Li, G., Qin, T., Chen, Y., Chu, F., 2017. Preparation and formation mechanism of size-controlled lignin nanospheres by self-assembly. Ind. Crops Prod. 100, 146–152.
Yan, Z., Liao, G., Zou, X., Zhao, M., Wu, T., Chen, Y., Fang, G., 2020. Size-controlled and super long-term stable lignin nanospheres through a facile self-assembly strategy from kraft lignin. J. Agric. Food. Chem. 68 (31), 8341–8349.
Yuan, T.-Q., Sun, S.-N., Xu, F., Sun, R.-C., 2011. Characterization of lignin structures and lignin–carbohydrate complex (LCC) linkages by quantitative 13C and 2D HSQC NMR spectroscopy. J. Agric. Food. Chem. 59 (19), 10604–10614.
Yue, X., Suopajärvi, T., Mankinen, O., Mikola, M., Mikkelson, A., Ahola, J., Hiltunen, S., Komulainen, S., Kantola, A.M., Telkki, V.-V., Liimatainen, H., 2020. Comparison of lignin fractions isolated from wheat straw using alkaline and acidic deep eutectic solvents. J. Agric. Food. Chem. 68 (51), 15074–15084.
Zhang, H., Liu, X., Fu, S., Chen, Y., 2019. Fabrication of light-colored lignin microspheres for developing natural sunscreens with favorable UV absorbability and staining resistance. Ind. Eng. Chem. Res. 58 (31), 13858–13867.
Zhao, C., Qiao, X., Shao, Q., Hassan, M., Ma, Z., 2020. Evolution of the lignin chemical structure during the bioethanol production process and its inhibition to enzymatic hydrolysis. Energy Fuels 34 (5), 5938–5947.

Zhao, W., Xiao, L.-P., Song, G., Sun, R.-C., He, L., Singh, S., Simmons, B.A., Cheng, G., 2017. From lignin subunits to aggregates: insights into lignin solubilization. Green Chem. 19 (14), 3272–3281.
Zhou, X., Huang, T., Liu, J., Gao, H., Bian, H., Wang, R., Huang, C., Sha, J., Dai, H., 2021. Recyclable deep eutectic solvent coupling sodium hydroxide post-treatment for boosting woody/herbaceous biomass conversion at mild condition. Bioresour. Technol. 320, 124327.
Zikeli, F., Ters, T., Fackler, K., Srebotnik, E., Li, J., 2016. Wheat straw lignin fractionation and characterization as lignin-carbohydrate complexes. Ind. Crops Prod. 85, 309–317.